sustainable chemistry

MDPI

Article

Copolymerization of a Bisphenol a Derivative and Elemental Sulfur by the RASP Process

Timmy Thiounn [1], Moira K. Lauer [1], Menisha S. Karunarathna [1], Andrew G. Tennyson [1,2] and Rhett C. Smith [1,*]

[1] Department of Chemistry, Clemson University, Clemson, SC 29634, USA; tthioun@clemson.edu (T.T.); mlauer@clemson.edu (M.K.L.); mkaruna@clemson.edu (M.S.K.); atennys@clemson.edu (A.G.T.)
[2] Department of Materials Science and Engineering, Clemson University, Clemson, SC 29634, USA
* Correspondence: rhett@clemson.edu

Received: 24 July 2020; Accepted: 1 September 2020; Published: 10 September 2020

Abstract: Fossil fuel refining produces over 70 Mt of excess sulfur annually from for which there is currently no practical use. Recently, methods to convert waste sulfur to recyclable and biodegradable polymers have been delineated. In this report, a commercial bisphenol A (BPA) derivative, 2,2′,5,5′-tetrabromo(bisphenol A) (**Br_4BPA**), is explored as a potential organic monomer for copolymerization with elemental sulfur by RASP (radical-induced aryl halide-sulfur polymerization). Resultant copolymers, **BAS_x** (x = wt% sulfur in the monomer feed, screened for values of 80, 85, 90, and 95) were characterized by thermogravimetric analysis, differential scanning calorimetry, and dynamic mechanical analysis. Analysis of early stage reaction products and depolymerization products support proposed S–C_{aryl} bond formation and regiochemistry, while fractionation of **BAS_x** reveals a sulfur rank of 3–6. Copolymers having less organic cross-linker (5 or 10 wt%) in the monomer feed were thermoplastics, whereas thermosets were accomplished when 15 or 20 wt% of organic cross-linker was used. The flexural strengths of the thermally processable samples (>3.4 MPa and >4.7 for **BAS_{95}** and **BAS_{90}**, respectively) were quite high compared to those of familiar building materials such as portland cement (3.7 MPa). Furthermore, copolymer **BAS_{90}** proved quite resistant to degradation by oxidizing organic acid, maintaining its full flexural strength after soaking in 0.5 M H_2SO_4 for 24 h. **BAS_{90}** could also be remelted and recast into shapes over many cycles without any loss of mechanical strength. This study on the effect of monomer ratio on properties of materials prepared by RASP of small molecular aryl halides confirms that highly cross-linked materials with varying physical and mechanical properties can be accessed by this protocol. This work is also an important step towards potentially upcycling BPA from plastic degradation and sulfur from fossil fuel refining.

Keywords: recyclable polymers; fossil fuel waste; sulfur; inverse vulcanization

1. Introduction

High sulfur-content materials (HSMs) are attractive alternatives to petrochemical polymers because they can be synthesized primarily from waste sulfur for which there are limited uses and HSMs have distinct physical and optical properties from those of typical polyolefins [1,2]. Sulfur–sulfur bonds can form in a thermally reversible fashion, so HSMs can also be thermally healable and recyclable thermoplastics, even when highly cross-linked, in which cases traditional organic polymers are thermosets [3–8]. Thus far, the inverse vulcanization route, which requires an olefin comonomer for reaction with elemental sulfur (Scheme 1A), has been the primary approach to preparing such HSMs [9]. Although inverse vulcanization was reported only a few years ago, its potential for facile production of versatile materials was quickly recognized. In a very short time, olefins derived

from petroleum [8–16], plant and animal sources [11,17–34] bacteria [28] and algae [35] have all proven to be successful monomers for the production of HSMs by inverse vulcanization. These HSMs have garnered significant attention for their potential as IR transparent lenses for thermal imaging [36], electrode materials [37,38] absorbents [11,13,39–41], fertilizers [18,22], and structural materials [29,42–46]. It would seem that inverse vulcanization's only limitation is that the organic comonomer must contain olefinic units.

Radical-induced aryl halide-sulfur polymerization (RASP, Scheme 1B) has recently emerged as another way to produce HSMs [47–49]. RASP employs an aryl halide as the comonomer with elemental sulfur, thus expanding the scope of potential monomers for HSM preparation beyond the olefins required for inverse vulcanization. Although 1,4-diiodobenzene [47], chlorolignin [48], and 2,4-dimethyl-3,5-dichlorophenol have been used in the RASP process, the extent to which the ratio of organic small molecules to sulfur influences the properties of the resultant HSMs has yet to be fully elucidated.

Herein, RASP of sulfur and a commercial monomer, 2,2′,4,4′-tetrabromo(bisphenol A) (**Br_4BPA**), is undertaken to produce **BAS_x** (where x = wt% sulfur in the monomer feed). **BAS_x** copolymers were prepared having four different monomer ratios, ranging from 80 to 95 wt% sulfur in the monomer feed. Characterizing these copolymers provides (1) insight into the influence of monomer ratio on properties in HSMs produced by RASP and (2) the first HSMs produced by RASP wherein there is no possibility for benzylic cross-linking to supplement cross-linking due to direct S–C_{aryl} bond-forming reactions. **BAS_x** materials range from thermosets to thermoplastics, and all of them form materials wherein polymeric sulfur is stabilized by its incorporation into a cross-linked network. The influence of monomer feed ratio on the processability, composition, thermal properties, and mechanical properties was evaluated, and the recyclability of remeltable materials was validated.

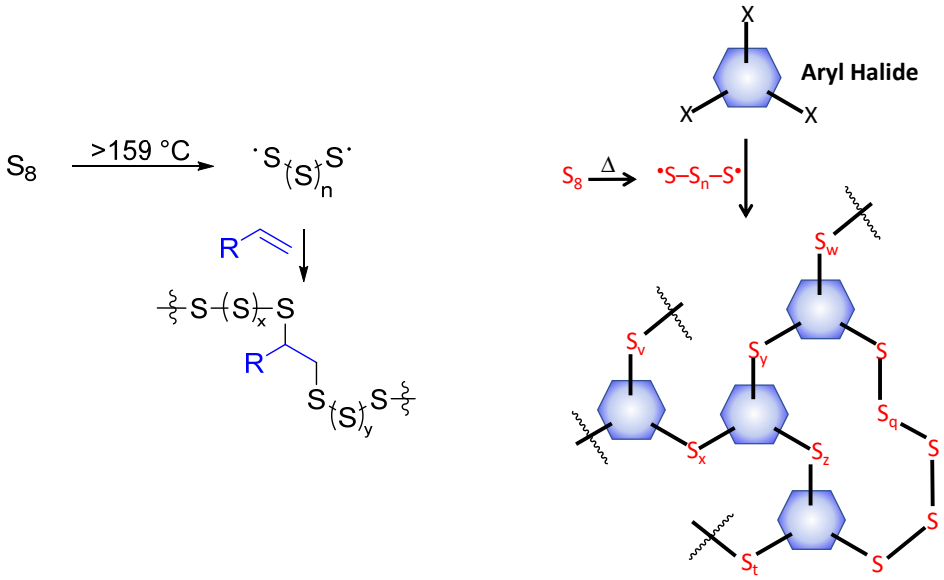

(**A**) Inverse Vulcanization of Alkenes (**B**) RASP of Aryl Halides

Scheme 1. Inverse vulcanization (**A**) and radical-induced aryl halide-sulfur polymerization (RASP) (**B**) routes to high sulfur-content materials (HSMs).

2. Results and Discussion

2.1. Synthesis and Structure

RASP proceeds by the Macallum mechanism whereby thermal reaction of aryl halides forms aryl radicals (Scheme 2A), generally at temperatures of ≥220 °C [48]. In the presence of excess sulfur, aryl radicals and halogen radicals rapidly react with elemental sulfur, leading to S–C_{aryl}

bond-formation and loss of the halogen as S_2X_2 (Scheme 2). The HSMs initially formed by this reaction contain oligomeric or polymeric sulfur chains that link aryl rings together. Such extended sulfur catenates are unstable and under ordinary conditions will revert back to an S_8 ring allotrope, so the end product of the Macallum polymerization is a poly(aryl sulfide) in which a single sulfur atom bridges aryl units. If a highly cross-linked network is present, however, the polymeric sulfur domains can be stabilized indefinitely. Stabilizing the polymeric sulfur domains is important for accessing materials with high mechanical strength, so establishing a highly cross-linked structure is a primary objective in selecting the organic monomer for RASP.

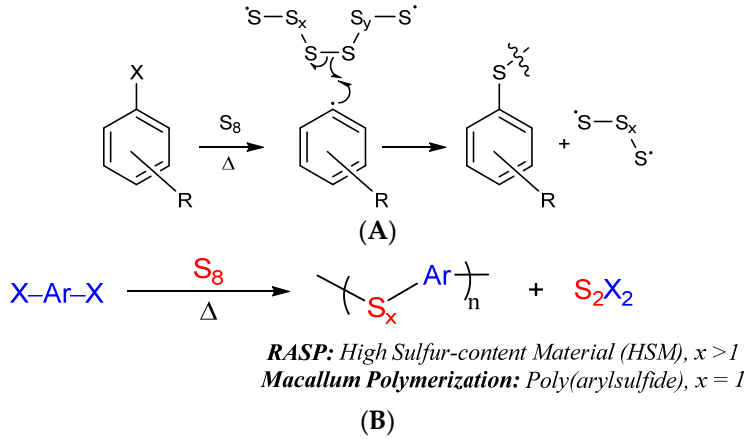

Scheme 2. The mechanism for S–C_{aryl} bond formation in Macallum polymerization/RASP ((**A**), X = Cl, Br or I) relies on thermal decomposition of sulfur and aryl halides, eventually leading to the net reaction (**B**).

In some prior demonstrations of RASP, a pre-existing polymeric network was supplied in the form of lignin [48,49], or a network comprised by a combination of S–$C_{benzylic}$ and S–C_{aryl} bonds was prepared. For the current work, an affordable aryl halide monomer that could form a highly cross-linked network comprised entirely from S–C_{aryl} bond-forming reactions (lacking the possibility for S–$C_{benzylic}$ cross links) was desired. A commercially available bisphenol A (BPA) derivative, 2,2′,5,5′-tetrabromo(bisphenol A) (**Br_4BPA**), was selected for this purpose. **Br_4BPA** should support a high cross-link density by merit of its ability to form up to four S–C_{aryl} cross-links per molecule, whereas the organic BPA subunit is a well-established and thermally stable structural element of durable polymers. Furthermore, the thermal reactivity of **Br_4BPA** under RASP conditions, a prerequisite for S–C_{aryl} bond formation as delineated in Scheme 2, has already been established [50].

As indicated in Scheme 2, the halogens are initially removed as S_2X_2 (X = Br in the current case), which are toxic and corrosive compound, so *caution should be exercised when performing the RASP reaction.* After reaction in the pressure tube, the tube should be fully cooled to room temperature before opening it in a fume hood, where S_2Br_2 in the product can be readily hydrolyzed by controlled reaction with water or slow reaction with humidity in the air. These RASP reactions can also be performed in a Schlenk flask vented to a water bath into which S_2Br_2 can be distilled as it forms, where it will be hydrolyzed to HX. Both the Schlenk flask and pressure tube methods prove effective for preparing the HSMs. Should the reaction be scaled up in the laboratory, trapping S_2Br_2 by its hydrolysis in a water bath as it forms could be an appropriate measure to prevent its release into the atmosphere. In the current context, at least some of the S_2Br_2 generated during RASP could also react with phenolic sites as well [51].

Another goal of the current research was to study the extent to which the monomer ratio influences thermal and mechanical properties of the resulting HSMs, something that has not been studied for RASP of small molecular aryl halides. Elemental sulfur and **Br_4BPA** were subjected to RASP by heating at 240 °C in a pressure tube. Four different sulfur monomer feeds, ranging from 80 to 95 wt%,

were employed to yield four copolymers **BAS$_x$** (where x = wt% sulfur in the monomer feed, Scheme 3). All of the materials have a dark brown-orange color characteristic of polymeric sulfur (Figure 1). Copolymers having ≥90 wt% sulfur in the monomer feed were remeltable, whereas **BAS$_{85}$** and **BAS$_{80}$** were thermosets. Although highly cross-linked polymers with structures comprising primarily C–C bonds are not generally remeltable in this way, the thermal processability of **BAS$_{90}$** and **BAS$_{95}$** is possible by merit of the thermal reversibility of S–S bond formation.

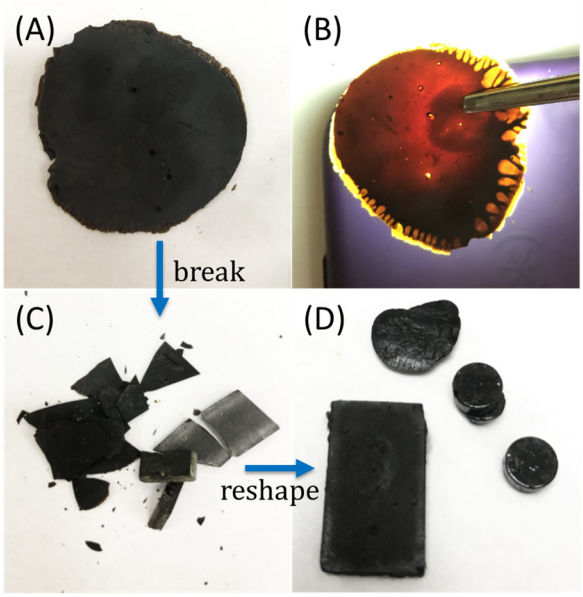

Figure 1. Although materials appear very dark under fluorescent room lighting (**A**), the brown-orange color characteristic of polymeric sulfur is evident in a backlit sample of **BAS$_{90}$** (**B**). The sample can be broken down (**C**), then readily remelted and recast (**D**).

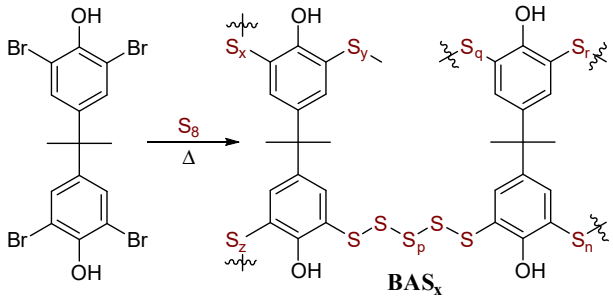

Scheme 3. Preparation of **BAS$_x$**.

The formulation of the **BAS$_x$** microstructure as being assembled via S–C$_{aryl}$ bond formation with the regiochemistry shown in Scheme 3 and in which the BPA backbone is intact is further supported by (1) analysis of depolymerization products and (2) reaction of **Br$_4$BPA** with smaller quantities of sulfur to give soluble products that could be analyzed by ^{1}H NMR spectrometry.

Quantification of S–C$_{aryl}$ bond formation was sought by analysis of depolymerization products of **BAS$_x$**. Depolymerization was affected by the reaction of **BAS$_x$** with $AlBr_3$ in toluene, a process that cleaves S–S bonds and S–C$_{alkyl}$ bonds while leaving S–C$_{aryl}$ bonds intact (Scheme 4A) [52,53]. After depolymerization and workup, one aryl thiol is produced for each C in a –C–S$_n$–C– unit for which $n \geq 2$. Any carbon atoms bridged by a single S atom will not be decomposed to thiols by this process. By quantifying the number of resulting thiols, the extent to which oligomeric/polymeric sulfur chains bridge carbon sites in the composite can thus be quantified. Quantification of thiols following depolymerization was undertaken by their reaction with Ellman's reagent, which produces

a selective colorimetric response to thiols that can be monitored by absorbance of the resultant thiolate at ~412 nm in the UV–VIS spectrum (Scheme 4B). The absorbance increase induced by exposure of Ellman's reagent to the depolymerization products allowed quantification of aryl thiols in the sample corresponding to 90% ± 10% of the available bromide sites in the **Br$_4$BPA** staring material. Elemental microanalysis for Br likewise revealed that 85–100% of the Br was removed following RASP.

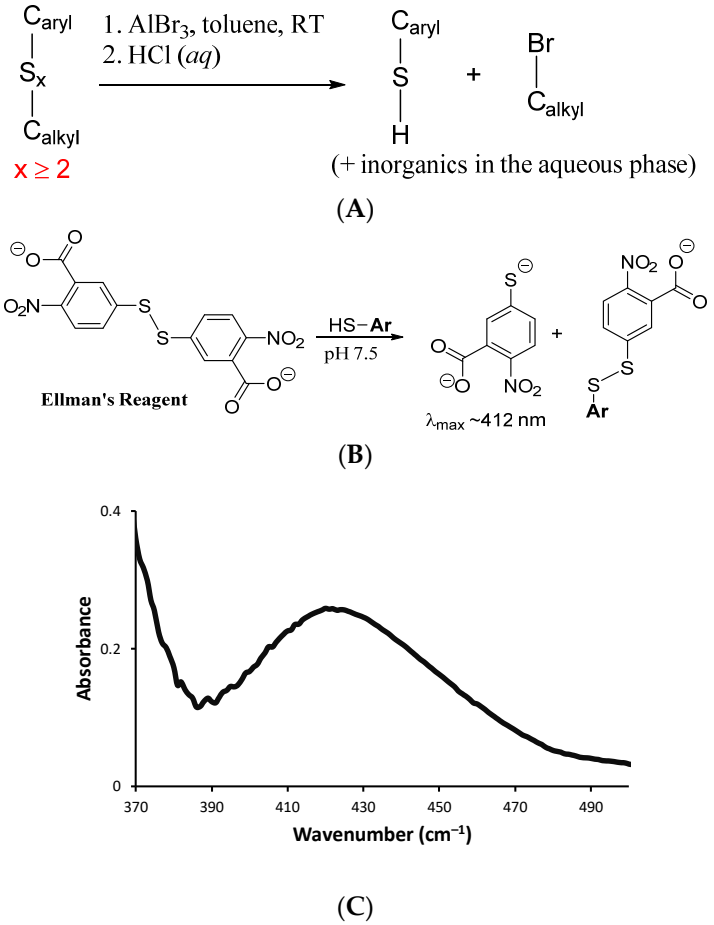

Scheme 4. (**A**) Reaction of $AlBr_3$ with aryl organosulfur compounds leads to formation of aryl thiols. (**B**) Ellman's reagent reacts with the resulting aryl thiols to give a colorimetric response. (**C**) UV spectrum from Ellman's analysis of products resulting from depolymerization of **BAS$_{90}$** by reaction with $AlBr_3$.

Next, the regiochemistry of S–C$_{aryl}$ bond formation was assessed by reacting **Br$_4$BPA** with 0.75 equivalent to S_8 under RASP conditions. If the RASP mechanism mirrors the Macallum mechanism in Scheme 2 initial formation of thiol **1** (Scheme 5A) would be expected after workup. Proton NMR spectrometric analysis of the product mixture (Scheme 5B) reveals that under these conditions, primarily one new aromatic resonance emerges at 7.74 ppm. Most of the starting material remains unreacted, with an aromatic resonance at 7.43 ppm. Compound **2** (Scheme 5C) appears to be the most similar model compound in the literature for which NMR data have been reported [54]. In this compound, a resonance at 7.66 ppm is attributable to proton H$_c$′, analogous to proton H$_c$ in **1** (at 7.74 ppm) that gives rise to the most prominent new signal in Scheme 5B. The resonance for H$_a$ is likely coincident with H$_c$ and the aryl protons on unreacted **Br$_4$BPA** because the influence of a thiol group and bromo group on a *m*-aryl proton are nearly identical. The resonance for the thiol proton, H$_d$, is observed at 5.64 ppm and its integration confirms its presence in the expected 1:1 ratio with H$_c$. Broadened resonances centered at around 7.2 and 8.6 ppm are attributed to the –OH protons H$_e$ and H$_f$, respectively. Although some minor resonances in the aromatic region were observed at about 7.55 and 7.40 ppm (and possibly

some overlapping the broad peak at 7.2 ppm), the predominant new species observed is consistent with the regiochemistry of S–C_{aryl} bond formation shown for **BAS$_x$** in Scheme 3. Further evidence that phenol functionalities are intact in the copolymers was provided by IR spectra, which reveal characteristic peaks at 3400 cm^{-1} (O–H stretch) and 1153 cm^{-1} (C–O stretch).

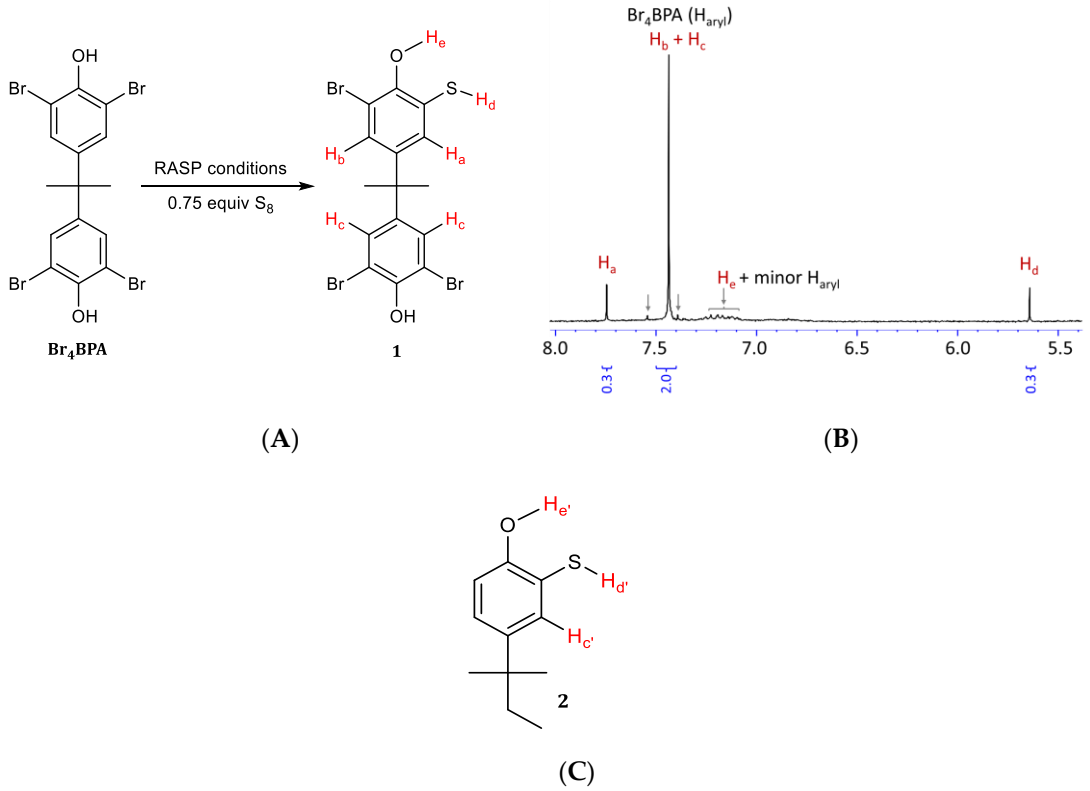

Scheme 5. Analysis of early reaction stage products of reaction between sulfur and **Br$_4$BPA**. The reaction (**A**) gives some of thiol **1**. (**B**) Proton NMR spectrum of crude reaction mixture containing thiol **1** and some Br_4BPA, as well as minor contributions from other unidentified aromatic species (indicated by arrows). Compound **2** (**C**) is the closest reported analogue of **1** that is reported in the literature for comparison.

The HSMs previously prepared by RASP contained some sulfur that was not covalently incorporated into the cross-linked network. Sulfur that is not covalently incorporated is readily extractable into CS_2, whereas highly cross-linked polymers are generally insoluble [8,28,55]. This provides a convenient way to fractionate such materials. **BAS$_x$** samples were thus fractionated in CS_2, and the relative masses of soluble and insoluble fractions were determined as shown in Table 1.

Elemental analysis of the CS_2-soluble fractions of **BAS$_x$** confirms that they consist of >98.5% sulfur. With the aforementioned data in hand, the sulfur rank (average number of sulfur atoms per cross-linking chain) can be calculated as follows. The number of carbon atoms cross-linked by sulfur (C_{xlink}) is known by subtracting the remaining bromine (from elemental analysis, Br_{ec}) from the initial amount of bromine in the reaction feed (Br_i). Fractionation data allowed for the calculation of the number of moles of sulfur atoms covalently incorporated (S_{cov}) into the materials by subtracting the free sulfur removed in the CS_2 wash (S_{fr}) from the total sulfur content (S_{add}). From these data, the sulfur rank (average number of sulfur atoms in each cross-linking chain) was calculated using Equation (1) (the factor of 2 is necessary because each sulfur chain must link to two carbon atoms to form a cross-link).

$$Sulfur\ Rank = 2 \times \left\{ \frac{S_{cov}}{C_{xlink}} \right\} = 2 \times \left\{ \frac{S_{add} - S_{fr}}{Br_i - Br_{ec}} \right\} \quad (1)$$

The sulfur ranks in **BAS$_x$** (Table 1) are similar to those found in materials prepared by RASP utilizing a dichloroxylenol derivative (sulfur rank = 5) [49] but lower than in materials prepared by RASP of a lignin derivative (12–31 sulfur atoms). The lower sulfur rank in **BAS$_x$** is expected on the basis of the high number of available cross-link sites. Similar sulfur ranks can also be obtained in HSMs prepared by inverse vulcanization. For example, inverse vulcanization HSMs wherein the olefin was a polystyrene derivative [8] or a tyrosine derivative [55] both have sulfur ranks of five. The number of available cross-link sites per sulfur in the copolymers appears to dictate the sulfur rank regardless of whether inverse vulcanization or RASP is used to prepare the material. Although the fractionation studies confirm the presence of sulfur that is not covalently bound to the cross-linked material, no phase separation was observed by scanning electron microscopy (SEM) with element mapping by energy-dispersive X-ray analysis (EDX), which confirmed uniform distribution of sulfur, carbon, and oxygen with almost no Br detectable (Figures S1 and S2 in the Electronic Supplementary Information).

Table 1. Fractionation and sulfur rank of **BAS$_x$**.

	Sulfur Rank	CS_2-Insoluble (%)	Sulfur Atoms Cross-Linking BPA Units (% of All S)
BAS$_{80}$	4 ± 1	28	20
BAS$_{85}$	3 ± 1	20	8
BAS$_{90}$	6 ± 1	17	5
BAS$_{95}$	5 ± 1	8	8

2.2. Thermal and Morphological Properties

HSMs can exhibit complex thermal behavior. Indeed, the S–S bonds in polymeric sulfur domains comprising important structural elements in HSMs undergo bond breakage at temperatures as low as ~90 °C. This S–S metathesis behavior has been exploited in innovative approaches to lower temperature processing of HSMs [56–59]. The labile nature of the S–S bonds allows for a variety of interesting thermal characteristics. Differential scanning calorimetry (DSC, Table 2 and Figures S3–S6 in the Electronic Supplementary Information) analysis of **BAS$_x$** revealed a number of notable morphological changes over the range of −60 to + 140 °C. The typical melt peak for sulfur domains of the materials was observed at 114–116 °C, slightly depressed from the melting point of pure orthorhombic sulfur. The presence of polymeric sulfur for all of the materials was also evident from the observation of the characteristic glass transition (T_g) at between −31 and −36 °C, consistent with the characteristic polymeric sulfur color of the materials (Figure 1). Determination of crystallization and melting enthalpies from the DSC data also allowed the quantification of the percent crystallinity of the composites. Crystallinity decreases predictably as more of the organic cross-linking unit is incorporated, to the extent that the crystallinity of **BAS$_{95}$** is only 40% that of sulfur despite being composed of 95 wt% sulfur. A primarily amorphous polymer is attained with 20 wt% of organic cross-linker in the monomer feed, as reflected in the 8% crystallinity of **BAS$_{80}$**.

Table 2. Thermal properties of $\mathbf{BAS_x}$.

	$\mathbf{BAS_{95}}$	$\mathbf{BAS_{90}}$	$\mathbf{BAS_{85}}$	$\mathbf{BAS_{80}}$
T_d [a] (°C)	240	222	233	231
Char Yield	2%	4%	7%	9%
T_g [b] (°C)	−36	−34	−35	−31
T_{cc} [c] (°C)	14, 41	25, 39	14, 38	39
T_m [d] (°C)	116	115	115	114
ΔH_m (J/g) [e]	30	28	28	21
ΔH_{cc} (J/g) [f]	7, 3	18, 1	16, 1	17
χ_c (%) [g]	40	20	20	8

[a] Determined from the onset of the major mass loss peak. [b] Determined from the onset of transition from the third heating cycle of the DSC curve. [c] Temperature at which cold crystallization peak maxima are observed. [d] Temperature of peak minimum for melting of sulfur domains. [e] The melting enthalpy for $\mathbf{BAS_x}$. [f] The cold crystallization enthalpy for $\mathbf{BAS_x}$. [g] The percent crystallinity of each sample calculated according to Equation (2).

The chemical instability of the polymer covalent bonds at the polymerization temperature (for either inverse vulcanization or RASP) would seem to be in conflict with the fundamental idea that polymerization must be carried out at a temperature below the decomposition point of the product. It is the dynamic nature of the S–S bonds that allows the higher temperature inverse vulcanization and RASP processes to be exploited to prepare HSMs. Thermogravimetric analysis (TGA) of $\mathbf{BAS_x}$ and of the $\mathbf{BAS_{90}}$ fraction from which free sulfur had been removed provide some additional insight into the thermal behavior of the composites.

Thermogravimetric analysis of $\mathbf{BAS_x}$ materials revealed onset of mass loss at between 222 and 240 °C (T_d in Table 2, traces provided in Figure S7 of the Electronic Supplementary Information), which is below the RASP reaction temperature. Thermal mass loss was attributed primarily to sulfur sublimation as would be expected of materials composed of 80–95 wt% sulfur heated in an open TGA pan. When a bulk sample of $\mathbf{BAS_{90}}$ is heated to 240 °C in a flask fitted with cold fingers, e.g., about 70 wt% of the material is collectable as sublimed sulfur. This is in contrast to heating during reaction in a sealed vessel from which escape of sulfur is not possible (this was confirmed by elemental analysis of the composites). Further evidence that thermal mass loss is primarily attributable to sublimation of sulfur was obtained by TGA analysis of the $\mathbf{BAS_{90}}$ fraction after sulfur removal, revealing a T_d value of 291 °C (Figure S8A in the Electronic Supplementary Information), well above the reaction temperature. Additionally, isothermal TGA revealed that the $\mathbf{BAS_{90}}$ sample from which free sulfur had been removed showed no major mass loss until after about 30 min of heating at 240 °C (Figure S8B in the Electronic Supplementary Information). This time scale provides some insight into the induction period required for thermally induced rearrangement of polymeric sulfur domains in $\mathbf{BAS_{90}}$ to form sublimable S_8.

2.3. Mechanical Properties

The remeltable samples, $\mathbf{BAS_{95}}$ and $\mathbf{BAS_{90}}$, can be fabricated into any number of shapes (Figure 1) by simply pouring the molten materials into a silicone mold and allowing the samples to harden upon cooling to room temperature. This allowed the two materials to be conveniently fabricated into rectangular prismatic beams appropriate for flexural strength analysis in a dynamic mechanical analyzer (Figures S9 and S10 in the Electronic Supplementary Information). The flexural strengths (Table 3) of both $\mathbf{BAS_{90}}$ (>3.4 MPa) and $\mathbf{BAS_{95}}$ (>4.7 MPa) are comparable to that of portland cement (3–5 MPa). It is notable that the flexural strength values reported in Table 3 represent lower limits to the flexural strengths of the $\mathbf{BAS_x}$ materials because the instrument was unable to apply enough stress to break the samples. In contrast, the portland cement sample of the same dimensions was broken by the instrument at a force corresponding to a flexural strength of 3.7 MPa. Portland cement is an important target for replacement by more sustainably sourced and recyclable materials because the

production of portland cement is energy intensive and is responsible for 8–12% of anthropogenic CO_2 emissions [60,61].

Table 3. Properties and acid resistance of $\mathbf{BAS_x}$.

	Flexural Modulus/Strength (MPa)	
	Before Acid	**After Acid** [a]
Portland cement	390/3.7	– [b]
$\mathbf{BAS_{90}}$	290/>4.7 [c]	300/>4.7 [c]
$\mathbf{BAS_{95}}$	360/>3.4 [c]	330/>3.4 [c]

[a] Acid challenge involved submerging the sample in 0.5 M H_2SO_4 for 24 h. [b] A portland cement sample decomposes under the acid challenge conditions. [c] The flexural strength value represents a lower limit to the strength because the instrument could not apply enough force to break the sample.

In addition to their potential for high strength, sulfur cements, including $\mathbf{BAS_x}$, exhibit very little water uptake (<3 mass %) compared to portland cement (28 mass %), making them more resistant to fissure formation resulting from repetitive freeze–thaw cycles. The density of $\mathbf{BAS_x}$ (1.8 g/cm^3) is also similar to that of portland cement (1.5 g/cm^3). One particularly attractive application space for sulfur cements like $\mathbf{BAS_x}$ is in low-pH environments, because HSMs have proven highly resistant to mechanical deterioration by acid [28,29,62,63]. Recent studies have shown, e.g., that cellulose–sulfur composites are impervious to degradation by sulfuric acid under conditions that completely dissolve a portland cement block of the same dimensions. $\mathbf{BAS_x}$ materials were likewise evaluated for their ability to withstand acid challenge by submerging samples in 0.5 M H_2SO_4 for 24 h. Both $\mathbf{BAS_{90}}$ and $\mathbf{BAS_{95}}$ maintained their dimensional integrity and flexural strength under these conditions, whereas the portland cement sample was completely decomposed (Table 3).

Having shown that $\mathbf{BAS_{90}}$ outperforms portland cement in flexural strength and acid resistance, the next test was to evaluate whether $\mathbf{BAS_{90}}$ material could be recycled. For this test, the flexural strength of a sample of $\mathbf{BAS_{90}}$ was determined after recursive cycles of pulverization, remelting, and curing in a silicone mold. The results of these measurements for seven cycles are shown in Figure 2. $\mathbf{BAS_{90}}$ maintains of its mechanical strength, as measured from its storage modulus at 25 °C, within measurement error after this process, although some of the recycling steps produced material with somewhat lower (90–80%) strength. This observation is consistent with some previous reports on the recyclability of HSMs, in which full strength was maintained even after over a dozen cycles [8,28]. The recyclability of HSMs by repetitive melt processing represent a significant improvement over some widely used petrochemical polymers like polyethylene terephthalate (PETE) [64]. The recyclability for PETE is dramatically diminished after only a few thermal processing cycles, to the extent that the strain-at-break falls from 42% for freshly manufactured samples to only 0.7% after only the fifth cycle [65]. Even if $\mathbf{BAS_x}$ can only be recycled four or five times while maintaining its mechanical durability, this would also be a marked improvement over portland cement, the vast majority of which is land filled at its end of life.

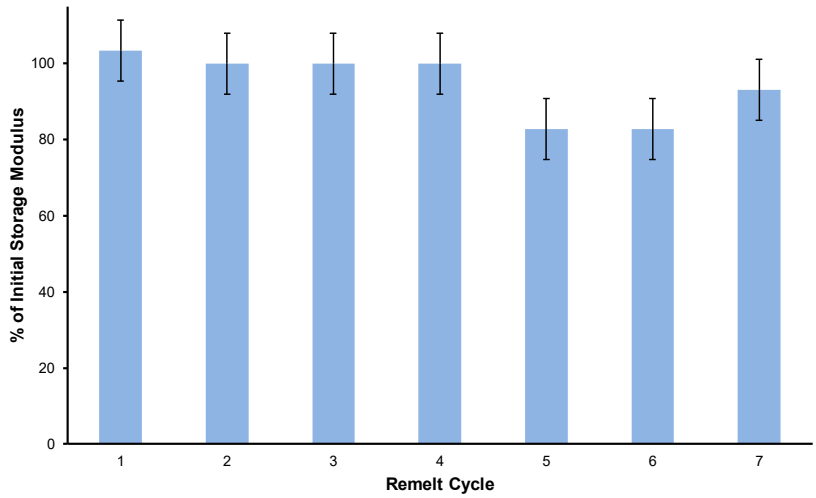

Figure 2. The percent storage modulus retained of **BAS_{90}** after seven pulverization/remelting/recasting cycles.

3. Conclusions

In conclusion, the first step to evaluating the influence of monomer feed on the properties of copolymers produced by RASP reveals that both thermosets and thermoplastics can be accomplished. RASP also proves effective at stabilizing polymeric sulfur within a network made exclusively by S–C_{aryl} bond-forming reactions, in a manner analogous to the stabilization of polymeric sulfur afforded in HSMs prepared by inverse vulcanization. The resultant copolymers have flexural strengths comparable to familiar commercial building materials like portland cement but have improved capabilities in terms of acid resistance and recyclability.

4. Experimental

4.1. Chemicals and Materials

Tetrabromobisphenol A (>98%) was purchased from TCI America. Sulfur powder (99.5%) was purchased from Alfa Aesar. These chemicals were used without further purification. All processes were carried out under ambient conditions unless otherwise specified.

4.2. General Considerations

Thermogravimetric analysis (TGA) data were recorded on a Mettler Toledo TGA 2STARe instrument over the range of 25–800 °C, with a heating rate of 5 °C min^{-1} under a flow of N_2 (20 mL min^{-1}). Differential scanning calorimetry (DSC) data was obtained using Mettler Toledo DSC 3 STAR^e System, over the range of −60 to 140 °C, with a heating rate of 5 °C min^{-1} under a flow of N_2 (200 mL min^{-1}). All the reported data were taken from the third heat/cool cycles.

Dynamic mechanical analysis (DMA) data was acquired using Mettler Toledo DMA 1 STAR^e System in single cantilever mode. DMA samples were cast from silicone resin molds (Smooth-On OOMOO®30 tin cure). The samples were cured for 120 h prior to stress–strain analysis at room temperature. The sample dimensions were approximately 40 mm × 11 mm × 2 mm and were clamped with 1 cN·m force. The samples cured for 120 h prior to stress–strain analysis at room temperature. The samples were clamped under single cantilever mode. The force was varied from 0 to 10 N with a ramp rate of 0.1 N·min^{-1}.

Percent crystallinity of the composites was determined by using Equation (2):

$$\chi_c = \left\{ \frac{\Delta H_{m(BAS_x)} - \Delta H_{cc(BAS_x)}}{\Delta H_{m(S)} - \Delta H_{cc(S)}} \right\} \times 100\% \quad (2)$$

where χ_c is the percentage crystallinity with respect to sulfur, ΔH_m is the melting enthalpy for the indicated material (sulfur or **BAS$_x$**), and ΔH_{cc} is the cold crystallization enthalpy of the indicated material.

4.2.1. Synthesis of BAS_{95}

Elemental sulfur (9.5 g) and **Br$_4$BPA** (0.5 g) was weighed directly into a pressure tube under inert environment. The tube was heated to 240 °C and heating was continued for 24 h with continuous stirring with a magnetic stir bar. The whole procedure was done under N_2 gas, giving quantitative yield of the material. Elemental combustion microanalysis calculated: C, 1.67; S, 95.00; H, 0.11%; Br, 2.94%. Found: C, 2.11; S, 96.43; H, 0.00; Br, 0.00%.

4.2.2. Synthesis of BAS_{90}

Elemental sulfur (9.0 g) and **Br$_4$BPA** (1.0 g) was weighed directly into a pressure tube under inert environment. The tube was heated to 240 °C and heating was continued for 24 h with continuous stirring with a magnetic stir bar. The whole procedure was done under N_2 gas. Elemental combustion microanalysis calculated: C, 3.31; S, 90.00; H, 0.22; Br, 5.88%. Found: C, 3.76; S, 95.40; H, 0.10; Br, 0.43%.

4.2.3. Synthesis of BAS85

Elemental sulfur (8.5 g) and **Br$_4$BPA** (1.5 g) was weighed directly into a pressure tube under inert environment. The tube was heated to 240 °C and heating was continued for 24 h with continuous stirring with a magnetic stir bar. The whole procedure was done under N_2 gas, giving quantitative yield of the material. Elemental combustion microanalysis calculated: C, 4.97; S, 85.00; H, 0.33; Br, 8.82%. Found: C, 6.32; S, 89.88; H, 0.22; Br, 0.28%.

4.2.4. Synthesis of BAS80

Elemental sulfur (8.0 g) and **Br$_4$BPA** (2.0 g) was weighed directly into a pressure tube under inert environment. The tube was heated to 240 °C and heating was continued for 24 h with continuous stirring with a magnetic stir bar. The whole procedure was done under N_2 gas, giving quantitative yield of the material. Elemental combustion microanalysis calculated: C, 6.63; S, 80.00; H, 0.44; Br, 11.75%. Found: C, 7.69; S, 87.84; H, 0.21; Br, 0.99%.

4.2.5. Preparation of Early Reaction Stage Products from Br4BPA

Elemental sulfur (0.088 g, 3.4×10^{-4} mol of S_8) and **Br$_4$BPA** (0.25 g, 4.6×10^{-4} mol) was weighed directly into a pressure tube under an inert atmosphere. The tube was heated to 240 °C and heating was continued for 24 h with continuous stirring with a magnetic stir bar. The whole procedure was done under N_2 gas. After 24 h, the pressure tube was taken off the heat and allowed to cool to room temperature. An aliquot of $LiAlH_4$ (2.5 equivalent with respect to sulfur) suspended in toluene (10 mL) was then added to the pressure tube under an inert atmosphere to facilitate transformation of any S–S linkages to S–H units. The mixture was quenched with 0.5 M HCl solution followed by extraction with dichloromethane (3 × 30 mL). The organic layer was dried over Na_2SO_4 and the solvent was evaporated under reduced pressure to yield a brown sticky solid. Efforts to separate the constituent compounds by preparative TLC were unsuccessful.

1. CAUTION: Heating elemental sulfur with organics can result in the formation of H_2S gas. H_2S is toxic, foul smelling, and corrosive. This reaction may also produce S_2Br_2, a toxic and reactive material.
2. CAUTION: Heating material in a sealed tube can generate high pressures. Use caution, and consult the manufacturer of the pressure apparatus used for safety guidance.

4.2.6. Depolymerization with AlBr3

The **BAS$_x$** sample (30 mg) was powdered and mixed with 60 mg of $AlBr_3$ in a glovebox under an atmosphere of dry N_2. The mixture of solid was suspended in 6 mL of anhydrous toluene for 30 min. At the end of the reaction time, the solvent was filtered and 5% (*v*/*v*) HCl:ethanol (5 mL) was added. Following three consecutive washes, the organic layer in toluene was separated out.

4.2.7. Procedure for the Reaction of Depolymerization Products with Ellman's Reagent

The procedure was carried out as previously reported. The stock solution of DTNB (5,5′-Dithio-*bis*-(2-nitrobenzoic acid)) was prepared by dissolving 40 mg of DTNB in 10 mL of DMSO. The solution was 100-fold diluted into 0.1 mM DTNB solution using Tris·HCl (*Tris*(hydroxymethyl)aminomethane hydrochloride) buffer solution at a pH of 7.4. A 1 mL aliquot of the solution containing depolymerized products and 19 mL of 0.1 mM DTNB were mixed together and then allowed to stand at room temperature for 2 min at room temperature. The samples were then analyzed using a Cary 50 UV–VIS spectrophotometer. The same procedure was carried out without adding $AlBr_3$ to confirm the absence of thiol groups in the initial sample as well as on a sample of **BAS$_x$** that had not been depolymerized to rule out the presence of surface thiols prior to depolymerization.

Supplementary Materials: The following are available online at http://www.mdpi.com/2673-4079/1/2/13/s1, Figure S1: Surface analysis of BAS90 by scanning electron microscopy (SEM) revealed a smooth surface consistent with those observed in high sulfur-content materials prepared by inverse vulcanization, Figure S2. Surface analysis of BAS90 by energy-dispersive X-ray (EDX) analysis revealed even distribution of sulfur (A), carbon (B), oxygen (C) and bromine (D) content on the polymer surface, Figure S3. Differential scanning calorimetry of BAS95, Figure S4. Differential scanning calorimetry of BAS90, Figure S5. Differential scanning calorimetry of BAS85, Figure S6. Differential scanning calorimetry of BAS80, Figure S7. TGA traces showing thermally-induced mass loss for monomer Br4BPA (red), BAS95 (blue), BAS90 (black), BAS85 (violet) and BAS80 (green) under nitrogen, Figure S8. TGA traces for the fraction of BAS90 from which free sulfur has been removed. In one experiment mass loss was monitored as the sample was heated from room temperature to 600 °C (A), and in another case mass loss was monitored as the temperature was held at 240 °C for 2.5 h (B), Figure S9. Stress strain curve of BAS95 pre (blue line) and post acid (red line) soak for 24 h. The dotted black lines are the extrapolations of the linear region, Figure S10. Stress strain curve of BAS90 pre (blue line) and post acid (red line) soak for 24 h. The dotted black lines are the extrapolations of the linear region.

Author Contributions: Conceptualization, R.C.S.; methodology, R.C.S. and T.T.; formal analysis, R.C.S., T.T., M.K.L. and M.S.K.; investigation, T.T., M.K.L. and M.S.K.; resources, R.C.S. and A.G.T.; data curation, R.C.S., T.T., M.K.L. and M.S.K.; writing—original draft preparation, R.C.S.; writing—review and editing, R.C.S., T.T., M.K.L. and M.S.K.; supervision, R.C.S.; funding acquisition, R.C.S. All authors have read and agreed to the published version of the manuscript.

Funding: This research was funded by the National Science Foundation grant number CHE-1708844.

Acknowledgments: The authors would like to thank the NSF for funding this work (CHE-1708844).

Conflicts of Interest: The authors declare no conflict of interest.

References

1. Zhang, Y.; Glass, R.S.; Char, K.; Pyun, J. Recent advances in the polymerization of elemental sulphur, inverse vulcanization and methods to obtain functional Chalcogenide Hybrid Inorganic/Organic Polymers (CHIPs). *Polym. Chem.* **2019**, *10*, 4078–4105. [CrossRef]
2. Chalker, J.M.; Worthington, M.J.H.; Lundquist, N.A.; Esdaile, L.J. Synthesis and Applications of Polymers Made by Inverse Vulcanization. *Top. Curr. Chem.* **2019**, *377*, 1–27.
3. Michal, B.T.; Jaye, C.A.; Spencer, E.J.; Rowan, S.J. Inherently Photohealable and Thermal Shape-Memory Polydisulfide Networks. *ACS Macro Lett.* **2013**, *2*, 694–699. [CrossRef]
4. Griebel, J.J.; Nguyen, N.A.; Namnabat, S.; Anderson, L.E.; Glass, R.S.; Norwood, R.A.; MacKay, M.E.; Char, K.; Pyun, J. Dynamic Covalent Polymers via Inverse Vulcanization of Elemental Sulfur for Healable Infrared Optical Materials. *ACS Macro Lett.* **2015**, *4*, 862–866. [CrossRef]
5. Amaral, A.J.R.; Pasparakis, G. Stimuli responsive self-healing polymers: Gels, elastomers and membranes. *Polym. Chem.* **2017**, *8*, 6464–6484. [CrossRef]

6. Arslan, M.; Kiskan, B.; Yagci, Y. Recycling and Self-Healing of Polybenzoxazines with Dynamic Sulfide Linkages. *Sci. Rep.* **2017**, *7*, 1–11. [CrossRef]
7. Takahashi, A.; Goseki, R.; Ito, K.; Otsuka, H. Thermally Healable and Reprocessable Bis(hindered amino)disulfide-Cross-Linked Polymethacrylate Networks. *ACS Macro Lett.* **2017**, *6*, 1280–1284. [CrossRef]
8. Thiounn, T.; Lauer, M.K.; Bedford, M.S.; Smith, R.C.; Tennyson, A.G. Thermally-Healable Network Solids of Sulfur-Crosslinked Poly(4-allyloxystyrene). *RCS Adv.* **2018**, *8*, 39074–39082. [CrossRef]
9. Chung, W.J.; Griebel, J.J.; Kim, E.T.; Yoon, H.; Simmonds, A.G.; Ji, H.J.; Dirlam, P.T.; Glass, R.S.; Wie, J.J.; Nguyen, N.A.; et al. The use of elemental sulfur as an alternative feedstock for polymeric materials. *Nat. Chem.* **2013**, *5*, 518–524. [CrossRef]
10. Hasell, T.; Smith, J.; Green, S.; Petcher, S.; Parker, D.; Zhang, B.; Worthington, M.J.H.; Wu, X.; Kelly, C.; Baker, T.; et al. Crosslinker Copolymerization for Property Control in Inverse Vulcanization. *Chem. Eur. J.* **2019**, *25*, 10433–10440.
11. Parker, D.J.; Jones, H.A.; Petcher, S.; Cervini, L.; Griffin, J.M.; Akhtar, R.; Hasell, T. Low cost and renewable sulfur-polymers by inverse vulcanization, and their potential for mercury capture. *J. Mater. Chem. A* **2017**, *5*, 11682–11692. [CrossRef]
12. Zhang, Y.; Pavlopoulos, N.G.; Kleine, T.S.; Karayilan, M.; Glass, R.S.; Char, K.; Pyun, J. Nucleophilic Activation of Elemental Sulfur for Inverse Vulcanization and Dynamic Covalent Polymerizations. *J. Polym. Sci. A* **2019**, *57*, 7–12. [CrossRef]
13. Lin, H.-K.; Lai, Y.-S.; Liu, Y.-L. Cross-Linkable and Self-Foaming Polysulfide Materials for Repairable and Mercury Capture Applications. *ACS Sustain. Chem. Eng.* **2019**, *7*, 4515–4522. [CrossRef]
14. Wreczycki, J.; Bielinski, D.M.; Anyszka, R. Sulfur/organic copolymers as curing agents for rubber. *Polymers* **2018**, *10*, 870. [CrossRef]
15. Zhang, Y.; Griebel, J.J.; Dirlam, P.T.; Nguyen, N.A.; Glass, R.S.; MacKay, M.E.; Char, K.; Pyun, J. Inverse vulcanization of elemental sulfur and styrene for polymeric cathodes in Li-S batteries. *J. Polym. Sci. Part A: Polym. Chem.* **2017**, *55*, 107–116. [CrossRef]
16. Diez, S.; Hoefling, A.; Theato, P.; Pauer, W. Mechanical and electrical properties of sulfur-containing polymeric materials prepared via inverse vulcanization. *Polymers* **2017**, *9*, 59. [CrossRef]
17. Herrera, C.; Ysinga Kristen, J.; Jenkins Courtney, L. Polysulfides Synthesized from Renewable Garlic Components and Repurposed Sulfur Form Environmentally Friendly Adhesives. *ACS Appl. Mater. Interfaces* **2019**, *11*, 35312–35318. [CrossRef]
18. Mann, M.; Kruger, J.E.; Andari, F.; McErlean, J.; Gascooke, J.R.; Smith, J.A.; Worthington, M.J.H.; McKinley, C.C.C.; Campbell, J.A.; Lewis, D.A.; et al. Sulfur polymer composites as controlled-release fertilizers. *Organic Biomol. Chem.* **2019**, *17*, 1929–1936. [CrossRef]
19. Lundquist, N.A.; Worthington, M.J.H.; Adamson, N.; Gibson, C.T.; Johnston, M.R.; Ellis, A.V.; Chalker, J.M. Polysulfides made from re-purposed waste are sustainable materials for removing iron from water. *RSC Adv.* **2018**, *8*, 1232–1236. [CrossRef]
20. Hoefling, A.; Lee, Y.J.; Theato, P. Sulfur-Based Polymer Composites from Vegetable Oils and Elemental Sulfur: A Sustainable Active Material for Li-S Batteries. *Macromol. Chem. Phys.* **2017**, *218*, 1600303. [CrossRef]
21. Qin, X.; He, Y.; Khan, S.; Zhang, B.; Chen, F.; Dong, D.; Wang, Z.; Zhang, L. Controllable Synthesis and Characterization of Soybean-Oil-Based Hyperbranched Polymers via One-Pot Method. *ACS Sustain. Chem. Eng.* **2018**, *6*, 12865–12871. [CrossRef]
22. Valle, S.F.; Giroto, A.S.; Klaic, R.; Guimaraes, G.G.F.; Ribeiro, C. Sulfur fertilizer based on inverse vulcanization process with soybean oil. *Polym. Degrad. Stab.* **2019**, *162*, 102–105. [CrossRef]
23. Worthington, M.J.H.; Shearer, C.J.; Esdaile, L.J.; Campbell, J.A.; Gibson, C.T.; Legg, S.K.; Yin, Y.; Lundquist, N.A.; Gascooke, J.R.; Albuquerque, I.S.; et al. Sustainable Polysulfides for Oil Spill Remediation: Repurposing Industrial Waste for Environmental Benefit. *Adv. Sustain. Syst.* **2018**, *2*, 1800024. [CrossRef]
24. Worthington, M.J.H.; Kucera, R.L.; Albuquerque, I.S.; Gibson, C.T.; Sibley, A.; Slattery, A.D.; Campbell, J.A.; Alboaiji, S.F.K.; Muller, K.A.; Young, J.; et al. Laying Waste to Mercury: Inexpensive Sorbents Made from Sulfur and Recycled Cooking Oils. *Chem. Eur. J.* **2017**, *23*, 16106. [CrossRef]
25. Crockett, M.P.; Evans, A.M.; Worthington, M.J.H.; Albuquerque, I.S.; Slattery, A.D.; Gibson, C.T.; Campbell, J.A.; Lewis, D.A.; Bernardes, G.J.L.; Chalker, J.M. Sulfur-Limonene Polysulfide: A Material Synthesized Entirely from Industrial By-Products and Its Use in Removing Toxic Metals from Water and Soil. *Angew. Chem. Int. Ed.* **2016**, *55*, 1714–1718. [CrossRef]

26. Fu, C.; Li, G.; Zhang, J.; Cornejo, B.; Piao, S.S.; Bozhilov, K.N.; Haddon, R.C.; Guo, J. Electrochemical Lithiation of Covalently Bonded Sulfur in Vulcanized Polyisoprene. *ACS Energy Lett.* **2016**, *1*, 115–120. [CrossRef]
27. Hoefling, A.; Nguyen, D.T.; Lee, Y.J.; Song, S.-W.; Theato, P. A sulfur-eugenol allyl ether copolymer: A material synthesized via inverse vulcanization from renewable resources and its application in Li-S batteries. *Mater. Chem. Front.* **2017**, *1*, 1818–1822. [CrossRef]
28. Karunarathna, M.S.; Lauer, M.K.; Thiounn, T.; Smith, R.C.; Tennyson, A.G. Valorization of waste to yield recyclable composites of elemental sulfur and lignin. *J. Mater. Chem. A* **2019**, *7*, 15683–15690. [CrossRef]
29. Lauer, M.K.; Estrada-Mendoza, T.A.; McMillen, C.D.; Chumanov, G.; Tennyson, A.G.; Smith, R.C. Durable Cellulose–Sulfur Composites Derived from Agricultural and Petrochemical Waste. *Adv. Sustain. Syst.* **2019**, *3*, 1900062. [CrossRef]
30. Smith, A.D.; Smith, R.C.; Tennyson, A.G. Carbon-Negative Polymer Cements by Copolymerization of Waste Sulfur, Oleic Acid, and Pozzolan Cements. *Sust. Chem. Pharm.* **2020**, *16*, 100249.
31. Smith, A.D.; Thiounn, T.; Lyles, E.W.; Kibler, E.K.; Smith, R.C.; Tennyson, A.G. Combining Agriculture and Energy Industry Waste Products to Yield Recyclable, Thermally Healable Copolymers of Elemental Sulfur and Oleic Acid. *J. Polym. Sci. Part A* **2019**, *57*, 1704–1710. [CrossRef]
32. Smith, A.D.; McMillin, C.D.; Smith, R.C.; Tennyson, A.G. Copolymers by Inverse Vulcanization of Sulfur with Pure or Technical Grade Unsaturated Fatty Acids. *J. Polym. Sci.* **2020**, *58*, 438–445. [CrossRef]
33. Lopez, C.V.; Karunarathna, M.S.; Lauer, M.K.; Maladeniya, C.P.; Thiounn, T.; Ackley, E.D.; Smith, R.C. High Strength, Acid-Resistant Composites from Canola, Sunflower, or Linseed Oils: Influence of Triglyceride Unsaturation on Material Properties. *J. Polym. Sci.* **2020**, *58*, 2259–2266. [CrossRef]
34. Lauer, M.K.; Karunarathna, M.S.; Tennyson, A.G.; Smith, R.C. Recyclable, Sustainable, and Stronger than Portland Cement: A Composite from Unseparated Biomass and Fossil Fuel Waste. *Mater. Adv.* **2020**, *1*, 590–594. [CrossRef]
35. Oishi, S.; Oi, K.; Kuwabara, J.; Omoda, R.; Aihara, Y.; Fukuda, T.; Takahashi, T.; Choi, J.-C.; Watanabe, M.; Kanbara, T. Synthesis and Characterization of Sulfur-Based Polymers from Elemental Sulfur and Algae Oil. *ACS Appl. Polym. Mater.* **2019**, *1*, 1195–1202. [CrossRef]
36. Griebel, J.J.; Namnabat, S.; Kim, E.T.; Himmelhuber, R.; Moronta, D.H.; Chung, W.J.; Simmonds, A.G.; Kim, K.-J.; van der Laan, J.; Nguyen, N.A.; et al. New Infrared Transmitting Material via Inverse Vulcanization of Elemental Sulfur to Prepare High Refractive Index Polymers. *Adv. Mater.* **2014**, *26*, 3014–3018. [CrossRef]
37. Chen, Z.; Droste, J.; Zhai, G.; Zhu, J.; Yang, J.; Hansen, M.R.; Zhuang, X. Sulfur-anchored azulene as a cathode material for Li-S batteries. *Chem. Commun.* **2019**, *55*, 9047–9050. [CrossRef]
38. Zhao, F.; Li, Y.; Feng, W. Recent Advances in Applying Vulcanization/Inverse Vulcanization Methods to Achieve High-Performance Sulfur-Containing Polymer Cathode Materials for Li-S Batteries. *Small Methods* **2018**, *2*, 1–34. [CrossRef]
39. Abraham, A.M.; Kumar, S.V.; Alhassan, S.M. Porous sulphur copolymer for gas-phase mercury removal and thermal insulation. *Chem. Eng. J.* **2018**, *332*, 1–7. [CrossRef]
40. Akay, S.; Kayan, B.; Kalderis, D.; Arslan, M.; Yagci, Y.; Kiskan, B. Poly(benzoxazine-co-sulfur): An efficient sorbent for mercury removal from aqueous solution. *J. Appl. Polym. Sci.* **2017**, *134*, 45306. [CrossRef]
41. Hasell, T.; Parker, D.J.; Jones, H.A.; McAllister, T.; Howdle, S.M. Porous inverse vulcanized polymers for mercury capture. *Chem. Commun.* **2016**, *52*, 5383–5386. [CrossRef] [PubMed]
42. Gregor, R.; Hackl, A. A new approach to sulfur concrete. *Adv. Chem. Ser.* **1978**, *165*, 54–78.
43. McBee, W.C.; Sullivan, T.A. Sulfur utilization in asphalt paving materials. *Adv. Chem. Ser.* **1978**, *165*, 135–160.
44. Vroom, A.H. Sulfur polymer concrete and its applications. *Polym. Concr. Int. Congr.* **1992**, *7*, 606–621.
45. Yu, S.; Kwon, H.; Noh, H.R.; Park, B.-I.; Park, N.K.; Choi, H.-J.; Choi, S.-C.; Kim, G.D. Preparation and characterization of a new cement-based composite with sulfur polymer. *RSC Adv.* **2015**, *5*, 36030–36035. [CrossRef]
46. Ksiazek, M.M.K. Evaluation of acid corrosion resistance of Portland cement composites impregnated with polymer sulfur composite. *Anti-Corros. Methods Mater.* **2017**, *64*, 1–15. [CrossRef]
47. Lee, J.M.; Noh, G.Y.; Kim, B.G.; Yoo, Y.; Choi, W.J.; Kim, D.-G.; Yoon, H.G.; Kim, Y.S. Synthesis of Poly(phenylene polysulfide) Networks from Elemental Sulfur and p-Diiodobenzene for Stretchable, Healable, and Reprocessable Infrared Optical Applications. *ACS Macro Lett.* **2019**, *8*, 912–916. [CrossRef]
48. Karunarathna, M.S.; Tennyson, A.G.; Smith, R.C. Facile new approach to high sulfur-content materials and preparation of sulfur-lignin copolymers. *J. Mater. Chem. A* **2020**, *8*, 548–553. [CrossRef]

49. Karunarathna, M.S.; Lauer, M.K.; Tennyson, A.G.; Smith, R.C. Copolymerization of an aryl halide and elemental sulfur as a route to high sulfur content materials. *Polym. Chem.* **2020**, *11*, 1621–1628. [CrossRef]
50. Barontini, F.; Marsanich, K.; Petarca, L.; Cozzani, V. The Thermal Degradation Process of Tetrabromobisphenol A. *Ind. Eng. Chem. Res.* **2004**, *43*, 1952–1961. [CrossRef]
51. Goud, D.R.; Pardasani, D.; Purohit, A.K.; Tak, V.; Dubey, D.K. Method for Derivatization and Detection of Chemical Weapons Convention Related Sulfur Chlorides via Electrophilic Addition with 3-Hexyne. *Anal. Chem.* **2015**, *87*, 6875–6880. [CrossRef]
52. Harnish, D.P.; Tarbell, D.S. Cleavage of the carbon-sulfur bond. Action of acid catalysts, especially aluminum bromide, on benzyl phenyl sulfide. *J. Am. Chem. Soc.* **1948**, *70*, 4123–4127. [CrossRef] [PubMed]
53. Tarbell, D.S.; Harnish, D.P. Cleavage of the carbon-sulfur bond in divalent sulfur compounds. *Chem. Rev.* **1951**, *49*, 1–90. [CrossRef]
54. Fleckenstein, C.; Denecke, H.; Fuchs, S.; Mueller, M.; Doering, M.; Cisielski, M.; Wagner, J.; Deglmann, P.; Nalawade, S.; Gutmann, P.; et al. Synthesis of Polyphenol Disulfides for Fireproofing Agents for Polymers. Patent 2013-EP55006, 2013135701, 20130312, 19 September 2013.
55. Thiounn, T.; Tennyson, A.G.; Smith, R.C. Durable, Acid-Resistant Copolymers from Industrial By-Product Sulfur and Microbially-Produced Tyrosine. *RSC Adv.* **2019**, *9*, 31460–31465. [CrossRef]
56. Lundquist, N.; Tikoalu, A.; Worthington, M.; Shapter, R.; Tonkin, S.; Stojcevski, F.; Mann, M.; Gibson, C.; Gascooke, J.; Karton, A.; et al. Reactive compression molding post-inverse vulcanization: A method to assemble, recycle, and repurpose sulfur polymers and composites. *Chem. Eur. J.* **2020**, *26*, 10035–10044. [CrossRef] [PubMed]
57. Zhang, B.; Gao, H.; Yan, P.; Petcher, S.; Hasell, T. Inverse vulcanization below the melting point of sulfur. *Mater. Chem. Front.* **2020**, *4*, 669–675. [CrossRef]
58. Zhang, B.; Petcher, S.; Hasell, T. A ternary system for delayed curing inverse vulcanisation. *Chem. Commun.* **2019**, *55*, 10681–10684. [CrossRef]
59. Westerman, C.R.; Jenkins, C.L. Dynamic Sulfur Bonds Initiate Polymerization of Vinyl and Allyl Ethers at Mild Temperatures. *Macromolecules* **2018**, *51*, 7233–7238. [CrossRef]
60. Khongprom, P.; Suwanmanee, U. Environmental benefits of the integrated alternative technologies of the portland cement production: Case study in Thailand. *Eng. J.* **2017**, *21*, 15–27. [CrossRef]
61. Chen, C.; Habert, G.; Bouzidi, Y.; Jullien, A. Environmental impact of cement production: Detail of the different processes and cement plant variability evaluation. *J. Clean. Prod.* **2010**, *18*, 478–485. [CrossRef]
62. Weber, H.H. New Applications and Expanding Markets for Sulphur Polymer Cement Concrete. *Am. Concr. Inst.* **1993**, *SP-137*, 49–72.
63. Weber, H.H.; McBee, W.C. New market opportunities for sulphur asphalt; Sulphur markets today and tomorrow. In Proceedings of the Biennial International Symposium, Washington, DC, USA, 9–13 February 2000; p. 24.
64. Thiounn, T.; Smith, R.C. Advances and approaches for chemical recycling of plastic waste. *J. Poly. Sci.* **2020**, *58*, 1347–1364. [CrossRef]
65. López, M.D.M.C.; Ares Pernas, A.I.; Abad López, M.J.; Latorre, A.L.; López Vilariño, J.M.; González Rodríguez, M.V. Assessing changes on poly(ethylene terephthalate) properties after recycling: Mechanical recycling in laboratory versus postconsumer recycled material. *Mater. Chem. Phys.* **2014**, *147*, 884–894. [CrossRef]